Spectrochimica Acta Part B 64 (2009) 961–967

Contents lists available at ScienceDirect

Spectrochimica Acta Part B

journal homepage: www.elsevier.com/locate/sab

Thermodynamic and spectroscopic properties of Nd:YAG–CO_2 Double-Pulse Laser-Induced Iron Plasmas ☆

Matthew Weidman, Santiago Palanco, Matthieu Baudelet, Martin C. Richardson *

Townes Laser Institute, CREOL – The College of Optics & Photonics, University of Central Florida, P.O. Box 162700, Orlando, FL 32816-2700, United States

ARTICLE INFO

Article history:
Received 15 December 2008
Accepted 27 July 2009
Available online 4 August 2009

Keywords:
Laser-induced breakdown spectroscopy
Double pulse LIBS
Laser ablation
Laser heating
Laser-induced particles

ABSTRACT

Double-Pulse Laser-Induced Breakdown Spectroscopy of iron using both Nd:YAG and TEA–CO_2 lasers has been investigated to better understand mechanisms of signal enhancement. The signal dependence on the delay between the two laser pulses shows an enhanced signal when the CO_2 laser pulse interacts with the sample before the Nd:YAG pulse. Signal kinetics and a simple model of sample heating by the CO_2 pulse show that the enhancement during the first 700 ns is due primarily to sample heating. Images of the sample surface after ablation as well as time-integrated pictures of the plasma suggest that particles are ejected from the surface during the first microseconds after the arrival of the CO_2 pulse and provide fuel for the subsequent plasma created by the Nd:YAG laser.

1. Introduction

Optical emission spectroscopy of laser-induced plasmas is a powerful spectroscopic diagnostic technique for sensing and other applications because of its ability to identify all types of materials (solid, liquid, gas), at a close distance as well as in a stand-off configuration. Despite the increasing popularity of this technique (also called LIBS — Laser-Induced Breakdown Spectroscopy) its sensitivity and precision are relatively poor compared to other well established analytical techniques. This is because of the uncertainty in laser energy coupling to the sample, significant matrix effects and relatively high background signal in the atomic and ionic spectra, among other reasons. One approach to improving sensitivity (by increasing the signal-to-continuum-background ratio) is the use of a double-pulse configuration (DP–LIBS). The aim of DP–LIBS is to improve the coupling of the laser energy to the target and to the ablated material, leading to a higher number of emitters from the analyzed sample in the plasma.

Since the first demonstration of double-pulse LIBS in 1969 by Piepmeier and Malmstadt [1], it has been demonstrated that two laser pulses for LIBS lead to enhanced emission intensities, longer plasma lifetimes and higher plasma temperatures. To optimize these effects, several combinations have been proposed involving various geometries (angle between the laser beams), different laser wavelengths and/or pulse durations and interpulse delay, as well as different pulse energies.

A collinear approach combines two pulses following the same path and focused upon the same point of the sample. The orthogonal configuration uses multiple optics to focus at different locations (double-focus collinear configuration has also been demonstrated [2]). Two configurations are possible with an orthogonal geometry: a pre-ablation spark to produce plasma above the sample prior to the ablation or a reheating spark focused upon the expanding plasma created by the first pulse.

From femtosecond to microsecond pulses, several combinations have been studied: fs–fs [3], fs–ns [4], ns–ns [5], ns–μs [6]. Other works have studied the influence of the combination of different wavelengths from ultraviolet (UV) to near- and mid-infrared (NIR and MIR): UV–NIR [5], Visible–NIR [8], NIR–NIR [5], NIR–MIR [6], NIR–MW [9] and the combination of pulses with different energy.

In Babushok et al. [10] and Scaffidi et al. [4], overviews of the different mechanisms leading to emission enhancement in DP–LIBS experiments are given. Depending on the delay time between the pulses, several explanations to the enhancement are given. From zero-delay to tens of ms, the physics behind the phenomenon changes. In Scaffidi et al., three mechanisms are mainly detailed: Pulse-plasma coupling (re-exciting or exciting of the plasma components), sample heating (heating by the hot plasma close to the surface resulting in increased ablation) and atmospheric effects (creation of a hot region with low density above the sample). In Babushok et al., an extensive list of possible effects is given from the preparation of the sample by the first pulse (smoothing, first crater, onset of melt) to the energy coupling with the plasma (ion yield, plasma re-heating, electron density).

☆ This paper was presented at the 5th International Conference on Laser-Induced Breakdown Spectroscopy (LIBS 2008), held in Berlin, Adlershof, Germany, 22–26 September 2008, and is published in the Special Issue of Spectrochimica Acta Part B, dedicated to that conference.

* Corresponding author.
E-mail address: mcr@creol.ucf.edu (M.C. Richardson).

0584-8547/$ – see front matter © 2009 Elsevier B.V. All rights reserved.
doi:10.1016/j.sab.2009.07.023

In this paper, we present the results of a double-pulse LIBS experiment where a nanosecond NIR pulse is combined with a MIR CO_2 laser pulse and focused on an iron sample. An 8-fold enhancement is reached by irradiating the sample first with the CO_2 laser pulse and then ablating it with the Nd:YAG laser. The effect of interpulse delay allows us to advance a combination of mechanisms leading to the enhancement of the LIBS signal compared to that obtained with a single Nd:YAG laser pulse.

2. Experimental setup

The experimental configuration is shown in Fig. 1. Two lasers are fired onto the same spot of a sample and the light emitted by the plasma is collected and guided to a spectrometer. The spatial overlap of the two pulses is shown on the inset in Fig. 1.

2.1. Laser sources

The Nd:YAG laser (Quantel Brilliant) is Q-switched and operated at the fundamental wavelength of 1064 nm. It is externally triggered at 0.33 Hz as limited by the CO_2 laser. A thin-film polarizer is used in conjunction with a λ/2 plate to provide continuous control of the laser energy from 5 mJ up to 340 mJ without changing the flashlamp voltage or the Q-switch delay time. The pulse energy is measured with a calibrated pyroelectric joulemeter (Gentec SOLO 2 with a QE-25 head). The peak-to-peak and RMS fluctuations in pulse energy are 1.51% and 0.44% respectively. The full width half maximum (FWHM) pulse duration is 5 ns as measured with a fast photodiode (Thorlabs) placed behind a dielectric turning mirror. The laser is focused with a 13.5 cm focal length lens at normal incidence, and the lens-to-sample distance is 13 cm. The beam radius at the sample location, determined by the knife-edge scan technique, is approximately 230 μm. The Nd:YAG laser was operated at 39 mJ per pulse, corresponding to an irradiance of 4.7×10^9 W/cm^2.

The CO_2 laser is a transversely excited atmospheric (TEA) CO_2 laser with components made by Lumonics. It utilizes an external 1 m half-symmetric resonator and emits at 10.6 μm. An intra-cavity iris is used to limit the number of higher order transverse modes and provide a circularly symmetric beam profile as viewed using an IR pyroelectric beam camera (Spiricon Pyrocam III). The laser energy is continuously tunable between 70 μJ and 80 mJ by using a set of crossed polarizers. The pulse energy is measured using the same pyroelectric joulemeter described above. The peak-to-peak and RMS fluctuations in pulse energy are 3.5% and 0.98%, respectively. The temporal profile is measured with a multiple junction photovoltaic detector (Vigo Systems PVM-10.6) with nanosecond response time. The temporal profile is composed of a 100 ns pulse followed by a 1 μs tail (Fig. 7a). The laser is focused with a 26 cm focal length lens at 13 degrees from normal, and the lens-to-sample distance is 25.5 cm. The beam radius at the sample location is approximately 280 μm as determined using a knife-edge scan. An irradiance of 30×10^6 W/cm^2 (assuming a pulse duration of 1 μs) was obtained with the laser operating at 75 mJ per pulse.

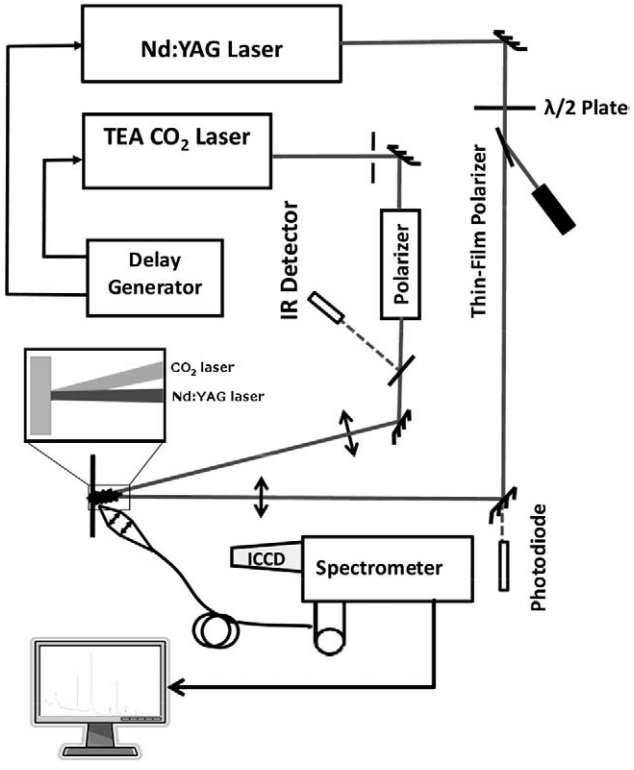

Fig. 1. Experimental setup.

2.2. Collection optics and spectrometer

The plasma emission is collected using an f/1 quartz lens and is coupled to a 1 m round-to-line UV-grade fiber bundle using a second (f/2) lens. The collection optics are at 40° from the surface normal. The fiber bundle is f-matched to a 0.5 m Czerny-Turner imaging spectrometer (Acton 2500i, Princeton Instruments) with a 1800 lines/mm grating. The light is detected using an intensified charge coupled device (Andor iStar DH720-25F-03) with 1024×256 pixels and a 25 mm Gen II intensifier. The intensifier delay is measured from the rising edge of the second pulse. Each spectrum is the average of 30 single acquisitions.

2.3. Timing

The timing of the experiment is controlled using two digital delay generators (Stanford Research Models DG-645 and DG-535). The DG-645 triggers the flashlamp of the Nd:YAG laser and also triggers the DG-535 at 10 Hz. The DG-535 divides the frequency to 0.33 Hz and triggers the Q-switch of the Nd:YAG laser, the CO_2 laser and the ICCD camera. Timing uncertainty between Nd:YAG and CO_2 pulses is primarily limited by the jitter in the CO_2 laser pulse onset and has peak-to-peak fluctuations of approximately 42 ns and a standard deviation of 9 ns. The timing configuration for the interpulse delay and the acquisition is shown in Fig. 2.

2.4. Samples

The target samples were a 100 μm-thick foil of 99.9 + % pure iron (Product #: 356808, Sigma-Aldrich, St. Louis, MO, USA). Each foil was cleaned with acetone and mounted so that it remained flat and vertical to minimize any deposition of material after the ablation. The

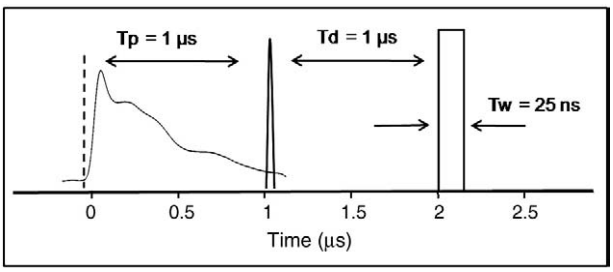

Fig. 2. Timing configuration of the experiment. The interpulse delay T_p is set as positive when the Nd:YAG laser precedes the CO_2 laser pulse and negative in the opposite order. The acquisition delay T_d is set to 1 μs after the second pulse and the duration of acquisition T_w to 25 ns.

sample was translated between each double pulse laser irradiation in order to present a fresh location for each shot.

3. Results and discussion

The original intention of this double-pulse LIBS study was to use 10.6 μm radiation from the CO_2 laser to re-heat or raise the temperature of the plasma created by the Nd:YAG laser after it had diffused away from the surface. Since the critical density of a plasma, the point at which light is reflected, scales as the square of the wavelength,

$$N_e^{cr} = \left(\frac{2\pi c}{e}\right)^2 \frac{\varepsilon_0 m_e}{\lambda^2}$$

longer wavelength light will interact with the plasma farther down the density gradient in the corona of the plasma produced by the Nd:YAG laser. With the relatively long scale lengths produced in the plasma, inverse Bremsstrahlung absorption (IBA) occurs at densities well below the critical density.

Previous studies using multiple wavelengths for double- pulse LIBS has been reported [5] using both UV and NIR pulses, and a correlation was found between signal enhancement and plasma temperature [5] showing that the signal increases with the temperature.

A comparison between single-pulse and double-pulse LIBS spectra is shown in Fig. 3. Each spectrum represents the average of 30 separate shots obtained with 1 μs delay (measured with respect to the second laser pulse) and an acquisition time of 25 ns. This acquisition time was chosen for determining instantaneous plasma temperature. Spectra for the single-pulse case of Nd:YAG and CO_2 are shown in a) and b) respectively, and the double-pulse case for Nd:YAG preceding the CO_2 pulse by 1 μs and Nd:YAG following the CO_2 pulse by 1 μs are shown in c) and d) respectively. In all cases, the energy of Nd:YAG and CO_2 lasers were 23 J cm^{-2} and 30 J cm^{-2} respectively.

The spectral lines in Fig. 3a are of singly-ionized iron. The weak signal in Fig. 3b can be attributed to minimal ablated mass and low plasma temperature during the relatively long interaction time of the CO_2 pulse. For the double pulse case, with the CO_2 laser pulse reheating the plasma (Fig. 3c), there is no signal enhancement relative to the signal acquired from the Nd:YAG only. This can be partially attributed to the acquisition delay time of 1 μs measured from the second laser pulse; therefore, 2 μs after the Nd:YAG pulse. This measurement does not imply significant plasma heating by the CO_2 pulse. However, the effects of plasma reheating using a CO_2 laser pulse (increased line intensities) have been demonstrated previously.

In work by Killinger et al. [6], an enhancement of both atomic (up to a factor of 60) and ionic (up to a factor of 300) aluminum lines for a high purity alumina sample was observed when a Nd:YAG pulse (5 ns, 50 mJ mm^{-2}) was followed by a CO_2 pulse (100 ns peak and 5 μs tail, 70 mJ mm^{-2}). The difference in behavior compared to our results can be attributed to both the different energy densities used, since the signal from a nanosecond laser plasma is approximately proportional to $I^{3/2}$ [7], I being the laser intensity, and sample properties. A metal sample was used in our case and an insulator in their case, each having different thermodynamic properties. A complete comparison cannot be made with our work since the timing configuration is not mentioned in their publication.

To understand the effect of the CO_2 pulse in double-pulse LIBS, the time delay between pulses has been varied from the CO_2 pulse preceding the Nd:YAG pulse by 5 ms to the CO_2 pulse following Nd:YAG pulse by 10 μs. For clarity, Fig. 4 shows the intensity of the Fe(II) 274.65 nm ionic line for a delay between −10 μs and +10 μs. A negative delay means the CO_2 pulse reaches the sample before the Nd:YAG pulse. Although there is no plasma reheating by the CO_2 pulse, a signal enhancement of approximately 8 times occurs for an interpulse delay of −1 μs. This signal enhancement is closely correlated to an enhancement in plasma temperature, as calculated using a Boltzmann plot [11] with the parameters listed in Table 1. The temperature for a

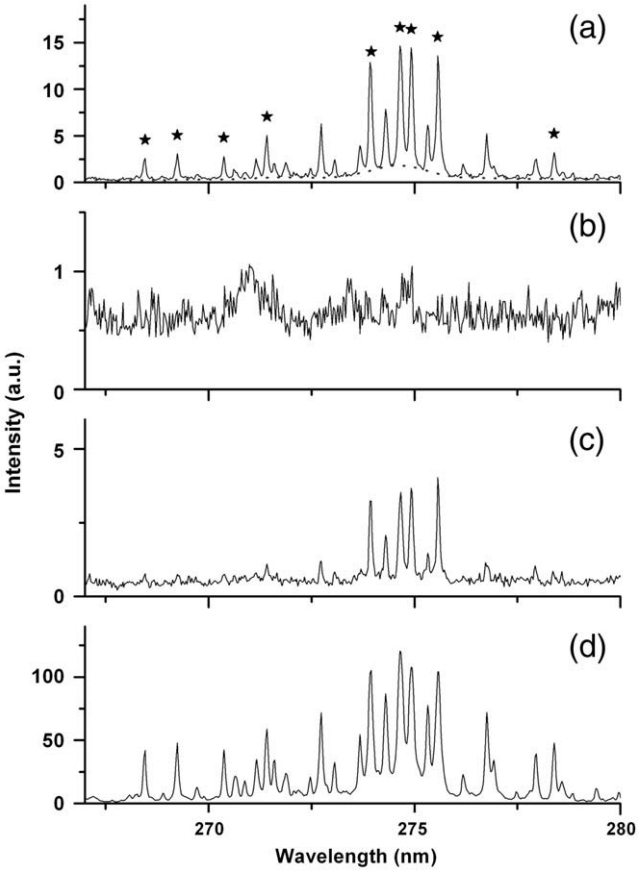

Fig. 3. LIBS spectra of iron from a) a single Nd:YAG pulse, b) a single CO_2 laser pulse, c) double pulse spectra with CO_2 following Nd:YAG by 1 μs compared with Nd:YAG alone LIBS spectrum and d) double pulse spectra with CO_2 preceding Nd:YAG by 1 μs. (Acquisition delay: 1 μs, duration of acquisition: 25 ns). In a), the dotted line shows a background spline interpolation and the stars indicate the lines used for plasma temperature calculation. Baseline correction is applied for all spectra.

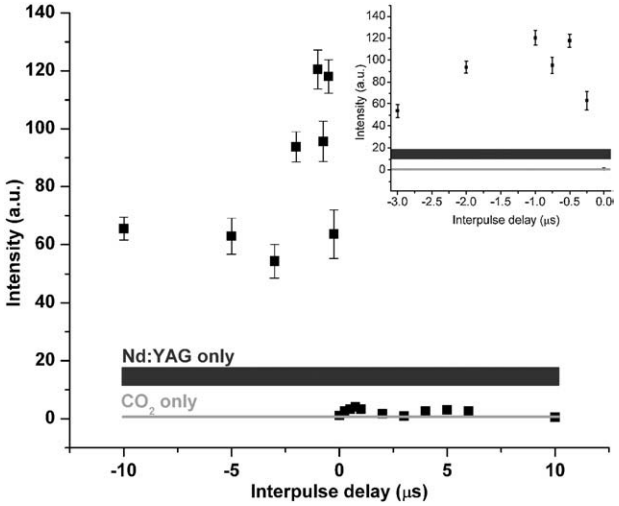

Fig. 4. Background-corrected peak intensity of the Fe II 274.65 nm line as a function of the interpulse delay. A negative delay means the CO_2 pulse reaches the samples before the Nd:YAG pulse. A positive delay is for the opposite timing configuration. Comparison is made with the single-pulse cases. The error bars represent the standard deviation over 30 single acquisitions. The inset in the upper right corner is a zoom between −3 μs and 0 μs showing the maximum enhancement at −1 μs.

Table 1
Parameters of the spectral lines used in the plasma temperature calculations [12].

Wavelength λ_{ul} (nm)	Upper level energy E_u (eV)	Degeneracy g_u	Transition probability A_{ul} (s^{-1})
268.48	8.43	10	$1.4\ 10^8$
269.26	8.37	12	$1.2\ 10^8$
270.40	7.97	8	$1.2\ 10^8$
271.44	5.55	6	$5.5\ 10^7$
273.96	5.51	8	$1.9\ 10^8$
274.65	5.59	6	$1.9\ 10^8$
274.93	5.55	8	$2.1\ 10^8$
275.57	5.49	10	$2.1\ 10^8$
278.37	7.70	10	$7.0\ 10^7$

single-pulse Nd:YAG plasma is $15\,000 \pm 2000$ K and $23\,000 \pm 2000$ K for double pulse with -1 μs interpulse delay.

When the CO_2 pulse is fired before the Nd:YAG, two mechanisms may occur: (i) the CO_2 pulse heats the sample before the arrival of the Nd:YAG pulse, (ii) the Nd:YAG interacts with the weak plasma created by the CO_2 pulse, ablating the sample softly and extracting non excited particles from the sample with size distribution ranging from atomic to clusters.

3.1. Heating of the sample by the CO_2 pulse

Several studies have shown a positive correlation between the intensity of the LIBS signal intensity and the sample temperature [13,14]. This phenomenon is explained by less energy being required to melt or vaporize the sample — the important parameters in long-pulse ablation above room temperature. Furthermore, the reflectivity of metals decreases when the surface temperature increases [15]. These two factors could lead to a better energy coupling between the Nd:YAG pulse and the sample if previously heated by the CO_2 pulse. To understand the importance of this phenomenon, a simple model of heat conduction is used.

The model is one-dimensional (1D) since the absorption length of a radiation with a 10.6 μm-wavelength at 298 K in the target is approximately 30 nm ($l_\alpha = 1/\alpha$, with $\alpha = 3.3\ 10^7\ m^{-1}$), which is much smaller than either laser beam diameter. The 1D heat equation has the following form:

$$\frac{\partial T(x,t)}{\partial t} = \frac{\partial}{\partial x}\left[\left(\frac{\kappa}{C_p\rho}\right)\frac{\partial T(x,t)}{\partial x}\right] + \frac{\alpha}{C_p\rho}S(x,t)$$

with $S(x,t) = I_0(t)e^{-\alpha x}(1-R)\cdot I_0(t)$ is the laser irradiance (in W cm^{-2}) and the other parameters are listed in Table 2. This calculation is done via a matricial implicit algorithm for solving parabolic partial differential equations [16]. The conditions of the algorithm are also given in Table 2. The temporal profile of the heat source $I_0(t)$ is an experimental profile acquired from a 75 mJ CO_2 pulse. The model yields an estimate of the temperature on the sample surface and doesn't include plasma shielding or ablation of the sample by the laser (the energy at the surface is considered completely transformed into heat). The lack of absorption of the laser pulse by the plasma leads us to consider that this simple model will give a higher estimate of the temperature at the surface of the sample. However, no conclusions on the ablation products or the plasma characteristics can be extracted.

Table 2
Physical and numerical parameters used in our 1D heat equation model.

Parameters	Values
Thermal conductivity, κ (W cm^{-1} K^{-1})	0.802
Specific heat, C_p(J g^{-1} K^{-1})	0.449
Mass density, ρ(g cm^{-3})	7.87
Absorption coefficient, α (m^{-1}) ($\lambda = 10.6$ μm)	$3.3\ 10^7$
Reflectivity, R ($\lambda = 10.6$ μm)	0.967
Melting point, T_m (K)	1811
Space range	$[x_0 = 0$ μm; $x_f = 10$ μm]
Space sampling	701 points
Time range	$[t_0 = -650$ ns; $t_f = 1849$ ns]
Time sampling	2500 points
Initial condition	$T(x,t=0) = 300K$
Boundary conditions on x_0 and x_f	$\frac{\partial T(x\,=\,x_0,t)}{\partial x} = 0$, $\frac{\partial T(x\,=\,x_f,t)}{\partial x} = 0$

The value corresponding to the solid form is given by the literature [19].

The calculated temperature distribution in the target is plotted as a function of time as shown in Fig. 5. The first conclusion is that the melting point T_m (1811 K for iron) is not reached with the irradiance of the CO_2 laser pulse used. The maximum temperature at the surface is approximately 860 K and occurs at 550 ns. This is supported by the microscope images of the sample irradiated by only the CO_2 laser (Fig. 6b) where small degradation of the material by the CO_2 pulse is observed after 30 shots on the same spot. The crater depth after 30 shots (using a Zygo NewView 6300 3D optical profiler) is not discernible within the roughness of the sample by the instrument and is smaller than the absorption length (30 nm) which is indicative of nanometric layers being ablated by each CO_2 pulse. Given minimal material removal by melting and vaporization, the Nd:YAG pulse following the CO_2 ablation is not influenced by significant sample deformation.

Given the maximum temperature occurs at $t = 550$ ns, a maximum signal enhancement at an interpulse delay of 1 μs is not completely explained by sample temperature effects.

3.2. Interaction of the Nd:YAG laser pulse with CO_2 laser induced plasma

With little apparent sample degradation as a result of the CO_2 laser, a continuum-like emission is detected as shown in Fig. 3b.

This continuum can be attributed to bremsstrahlung and/or poly-atomic clusters. These emitters are extracted by the CO_2 laser pulse during the interaction with the surface, when a nanometric layer is ablated. When the laser removes material from the surface, the size distribution of particles is limited by the absorption depth $1/\alpha$ [17]. Two types of emitters are localized in time-integrated pictures of the plasma in the visible region shown in Fig. 7b (using a manually triggered Nikon D40x DSLR with 300 mm 1:1 macro zoom lens at f/8 with 1 to 2 second exposure time to integrate the entire plasma lifetime). Light emission is observed at two different locations: one component along the normal and the other close to the surface. The paraxial emission can be attributed to small emitters (atoms and ions), ejected with high speed from the sample (tens of

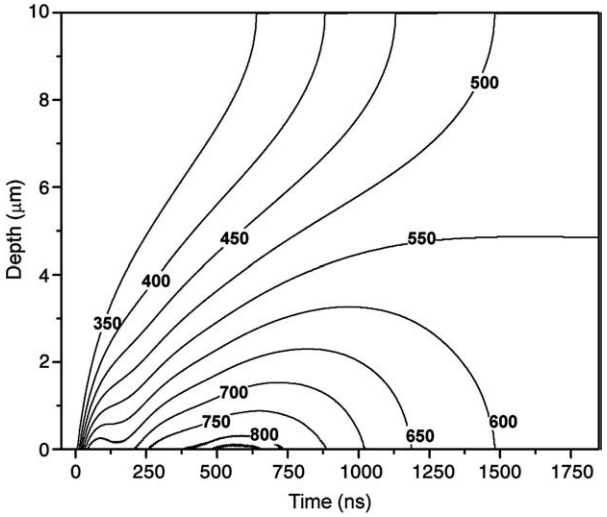

Fig. 5. Calculated temperature distribution in the target as a function of time for an iron sample after the irradiation with the laser pulse depicted in Fig. 7a. (see physical and algorithmic parameters in Table 1).

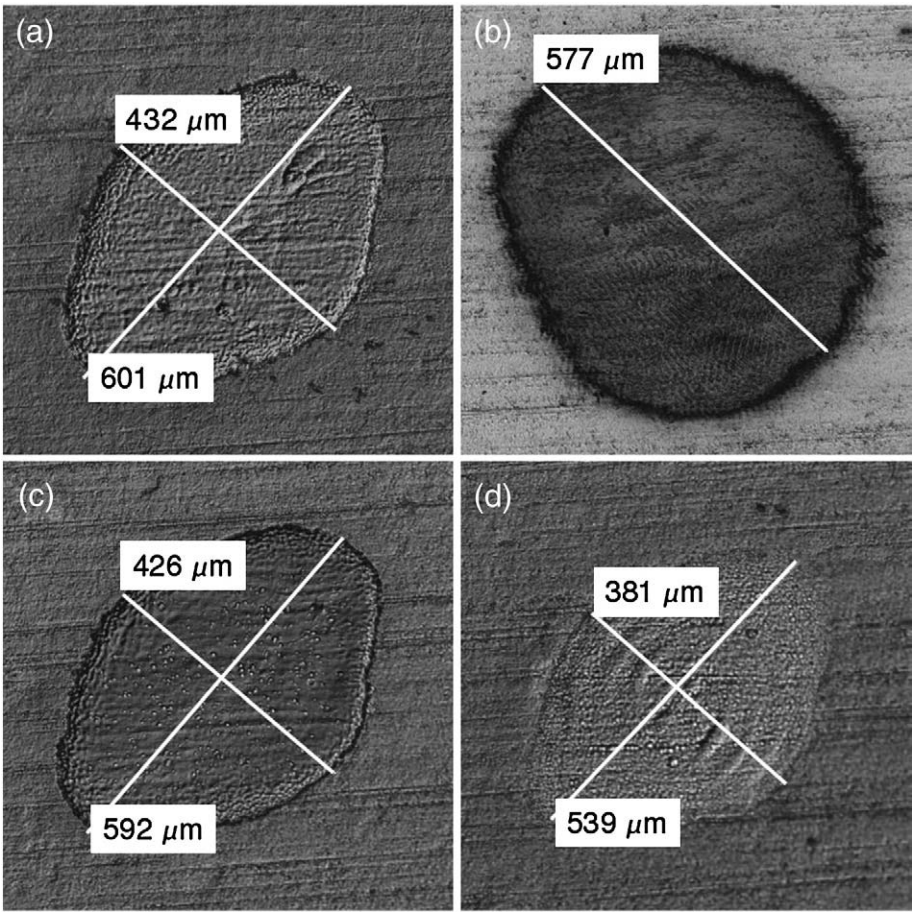

Fig. 6. Microscope pictures of the iron sample after a) a single Nd:YAG laser shot, b) an accumulation of 30 CO_2 laser shots, c) a combination of a Nd:YAG laser shot followed by a CO_2 laser shot 1 μs later and d) a combination of a CO_2 laser shot followed by a Nd:YAG laser shot 1 μs later.

km s^{-1}) [18], whereas the marginal emission can be due to slow heavy emitters (clusters) (hundreds of m s^{-1}) [18]. This spatially divided emission is compared with the light emission of the plasma created by the Nd:YAG laser only (acquired in the same conditions) where the plasma is homogeneously confined to the surface and its expansion is comparable to the beam waist.

The spatially integrated temporal trace of the visible emission is shown in Fig. 8c. The first peak is due to bremsstrahlung from electronic collisions with fast emitters, and is shown by the paraxial emission in Fig. 7b. During the course of the CO_2 laser pulse, there is a second emission increase peaking at 800 ns. This is attributed to heavy particles extracted from the surface during the relatively long CO_2 pulse evolution. The low velocity of these emitters restricts their position to within hundreds of microns of the sample, as seen in Fig. 7b.

When the Nd:YAG pulse arrives 1 μs after the CO_2 pulse, a maximum coupling with the CO_2 induced plasma occurs because the maximum number of particles has been extracted from the sample (since there is no excitation by the CO_2 laser anymore). Particle ablation by the Nd:YAG laser is efficient because of their high surface-to-mass ratio, and at this time an enhanced ionic LIBS spectrum is observed (Fig. 3d) compare to the surface ablation by the Nd:YAG only (Fig. 3a). There is a significant difference in the visible emission for the case of CO_2 pulse preceding the Nd:YAG pulse by 1 μs and the CO_2 pulse following the Nd:YAG pulse by 1 μs as reflected in Fig. 7c and d. These images show a less intense surface plasma in the second case suggesting the absorption of the Nd:YAG above the surface. This is also observed in the crater images shown in Fig. 6. The edges of the crater induced by the Nd:YAG in the double pulse case of CO_2 first are smoother than in the case when a single Nd:YAG pulse reaches the sample first (Fig. 6a and c).

3.3. Combination of mechanisms for LIBS signal enhancement

Maximum signal enhancement occurs when the CO_2 precedes the Nd:YAG pulse by 1 μs. This condition is shown in Fig. 8 along with the normalized plasma emission and calculated surface temperature. We can divide the timescale in two stages:

3.3.1. The first 700 ns

During the first 700 ns, there is a strong correlation between the surface temperature and the plasma emission. The 100 ns peak of the CO_2 laser pulse quickly heats the sample from approximately 300 K to 650 K. The tail of the pulse reaches a hot surface and heats the sample to 860 K. The signal follows the same trend until approximately 700 ns. This enhances the production of emitting products. These products are mainly heavy emitters rather than ions or atoms common to most LIBS plasmas and there is little surface modification, leading to the conclusion that these heavy particles have nanometer size. When the Nd:YAG pulse reaches a hot surface, less energy is needed for ablation resulting in increased mass ablation and LIBS signal.

3.3.2. Between 700 ns and 10 μs

The extraction of particles from the surface increases until approximately 0.7 to 1 μs. At this time, the coupling between the CO_2 induced plasma and the Nd:YAG pulse is maximum. Emission from the ablation of particles with a distribution of velocity around 500 m per second will remain within the field of view (approximately 2 mm) for approximately 4 μs. However, noticeable enhancement of the LIBS signal occurs until 10 μs. Further experiments are in progress to better explain the mechanisms of such a long enhancement.

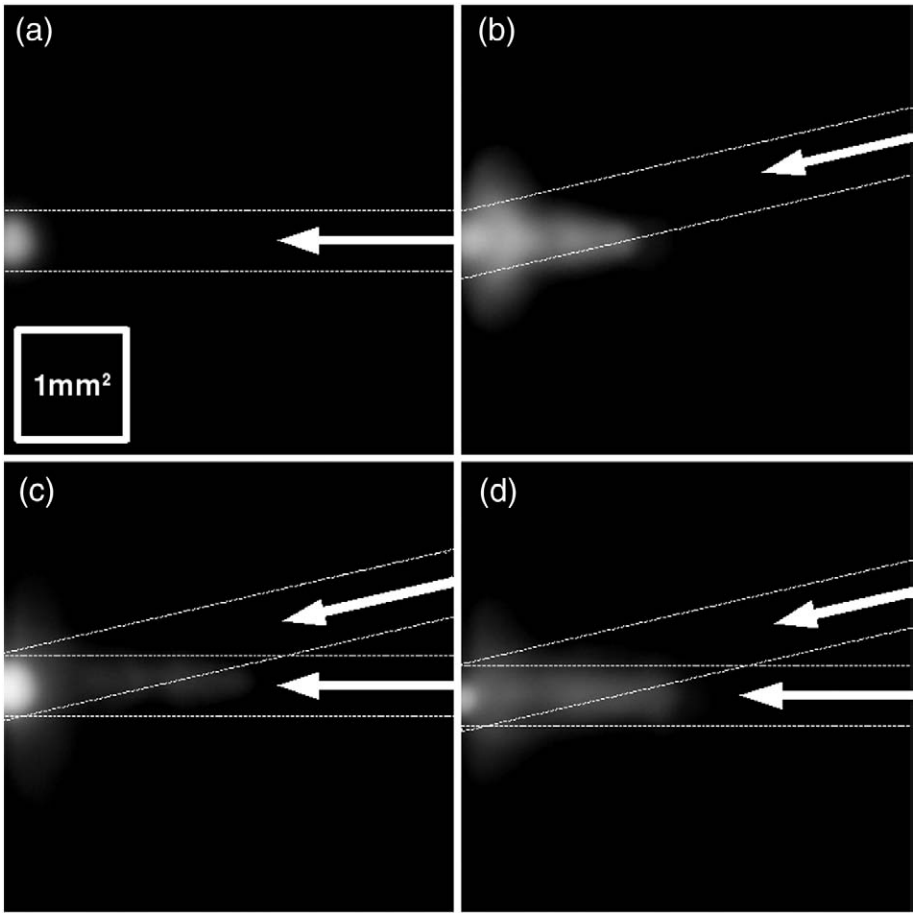

Fig. 7. Time-integrated pictures of the plasma produced by a) a single Nd:YAG laser shot, b) a single CO_2 laser shot, c) a combination of an Nd:YAG laser shot followed by a CO_2 laser shot 1 μs later and d) a combination of a CO_2 laser shot followed by a Nd:YAG laser shot 1 μs later. The arrows represent the direction of the incoming laser and the dotted lines the laser beam diameter $2w_0$.

4. Conclusion

The optical emission from laser-induced plasma in a double-pulse LIBS experiment (Nd:YAG at 1064 nm and CO_2 laser at 10.6 μm) on iron has been studied to understand which mechanisms are responsible for signal enhancement in this configuration. The CO_2 laser pulse heats the sample before the arrival of the Nd:YAG laser pulse during the first 700 ns, without melting the sample or creating noticeable surface deformation. Nevertheless, the bright continuum emission representative of heavy and slow moving particles extracted and ejected during the CO_2 laser interaction with the iron sample. These particles act as fuel for the second pulse, and lead to greatest signal enhancement approximately one microsecond after the beginning of the CO_2 laser pulse.

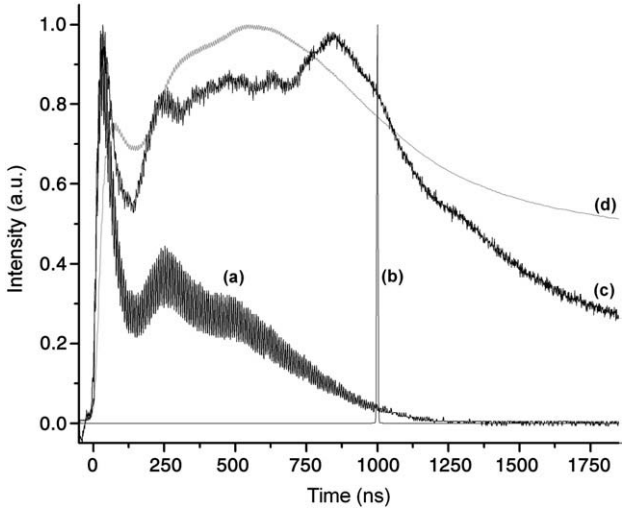

Fig. 8. Optimal timing for the maximum of LIBS signal enhancement: a) CO_2 laser pulse intensity, b) Nd:YAG laser intensity, c) the plasma emission from the CO_2 pulse only and d) the calculated surface temperature of the sample.

Acknowledgments

This work is supported by the US ARO-MURI program on "Ultrafast Laser Interaction Processes for LIBS and other Sensing Technologies", and by the State of Florida.

References

[1] E.H. Piepmeier, H.V. Malmstadt, Q-Switched laser energy absorption in the plume of an aluminum alloy, Anal. Chem. 41 (1969) 700–707.
[2] J. Bruce III, Alexander Dennis, Collinear dual pulse-dual focus enhancement of femtosecond LIBS, 5th International Conference on Laser-Induced Breakdown Spectroscopy (Berlin, Germany, 2008), 2008, 22–26 September.
[3] V. Pinon, C. Fotakis, G. Nicolas, D. Anglos, Double pulse laser-induced breakdown spectroscopy with femtosecond laser pulses, Spectrochim. Acta Part B 63 (2008) 1006–1010.
[4] J. Scaffidi, S.M. Angel, D.A. Cremers, Emission enhancement mechanisms in dual-pulse LIBS, Anal. Chem. 78 (1969) 24–32.
[5] L. St-Onge, V. Detalle, M. Sabsabi, Enhanced laser-induced breakdown spectroscopy using the combination of fourth-harmonic and fundamental Nd:YAG laser pulses, Spectrochim. Acta Part B 57 (2002) 121–135.
[6] D.K. Killinger, S.D. Allen, R.D. Waterbury, C. Stefano, E.L. Dottery, Enhancement of Nd:YAG LIBS emission of a remote target using a simultaneous CO_2 laser pulse, Opt. Express 15 (2007) 12905–12915.

[7] S. Palanco, C. López-Moreno, J.J. Laserna, Design, construction and assessment of a field-deployable laser-induced breakdown spectrometer for remote elemental sensing, Spectrochimica Acta Part B 61 (2006) 88–95.
[8] C. Gautier, P. Fichet, D. Menut, J.-L. Lacour, D. L'Hermite, J. Dubessy, Study of the double-pulse setup with an orthogonal beam geometry for laser-induced breakdown spectroscopy, Spectrochim. Acta Part B 59 (2004) 975–986.
[9] B. Kearton, Y. Mattley, Laser-induced Breakdown spectroscopy — sparking new applications, Nat. Photonics 2 (2008) 537–540.
[10] V.I. Babushok, F.C. DeLucia Jr., J.L. Gottfried, C.A. Munson, A.W. Miziolek, Double pulse laser ablation and plasma: laser induced breakdown spectroscopy signal enhancement, Spectrochim. Acta Part B 61 (2006) 999–1014.
[11] D.A. Cremers, L.J. Radziemski, Handbook of laser-induced breakdown spectroscopy, John Wiley & Sons Ltd, Chichester, 2006.
[12] Y. Ralchenko, A.E. Kramida, J. Reader and NIST ASD Team (2008). NIST Atomic Spectra Database (version 3.1.5), [Online]. Available: http://physics.nist.gov/asd3 [2008, December 2]. National Institute of Standards and Technology, Gaithersburg, MD.
[13] S. Palanco, L.M. Cabalín, D. Romero, J.J. Laserna, Infrared laser ablation and atomic emission spectrometry of stainless steel at high temperatures, J. Anal. At. Spectrom. 14 (1999) 1883–1887.
[14] S.H. Tavassoli, A. Gragossian, Effect of sample temperature on laser-induced breakdown spectroscopy, Opt. Laser Technol. 41 (2009) 481–485.
[15] M. von Allmen, A. Blatter, Laser-beam interactions with materials — physical principles and applications, 2nd edition, Springer, Berlin, 1998.
[16] J.P. Nougier, Méthodes de calcul numérique, 3rd edition, Masson, Paris, 1985.
[17] E.N. Sobol, Phase transformations and ablation in laser-treated solids, John Wiley & Sons, New York, 1995.
[18] S. Noel, J. Hermann, T.E. Itina, Nanoparticle generation in plasmas produced by ultra-short laser pulses, Appl. Surf. Sci. 253 (2007) 6310–6315.
[19] D.R. Lide, Handbook of chemistry and physics, 82nd edition, CRC Press, New York, 2001.